International Journal of Women's Health

Dovepress
Taylor & Francis Group

Open Access Full Text Article

ORIGINAL RESEARCH

A Dual-Sequence MRI-Based Radiomics Model for Predicting High-Intensity Focused Ultrasound Ablation Efficacy in Adenomyosis Treatment

Mengmeng Sun[1,2,*], Xinyi Deng[3,*], Hui Xing[1,4], Rui Zhang[3], Bingbing Fu[1], Tao Ai[5], Fang Wang[6], Xuechun Wang[6], Lei Chen[6], Xiaogang Mao[1,4], Feng Wu[3]

[1]Department of Obstetrics and Gynecology, Xiangyang Central Hospital, Affiliated Hospital of Hubei, University of Arts and Science, Xiangyang, People's Republic of China; [2]School of Medicine, Wuhan University of Science and Technology, Wuhan, People's Republic of China; [3]Department of Radiology, Xiangyang Central Hospital, Affiliated Hospital of Hubei University of Arts and Science, Xiangyang, People's Republic of China; [4]Hubei Provincial Clinical Research Center for Cervical Lesions, Xiangyang, People's Republic of China; [5]Department of Radiology, Tongji Hospital, Tongji Medical College, Huazhong University of Science and Technology, Wuhan, People's Republic of China; [6]Department of Research and Development, United Imaging Intelligence, Shanghai, People's Republic of China

*These authors contributed equally to this work

Correspondence: Feng Wu; Xiaogang Mao, Department of Radiology, Xiangyang Central Hospital, Affiliated Hospital of Hubei University of Arts and Science, No. 136 Jinzhou Road, Xiangyang, Hubei, 441021, People's Republic of China, Email wufeng@hbuas.edu.cn; tjmumxg@163.com

Purpose: The aim of this study is to develop a predictive model for the therapeutic efficacy of high-intensity focused ultrasound (HIFU) ablation in the treatment of adenomyosis, utilizing dual-sequence MRI radiomics.

Methods: A retrospective analysis was conducted on 114 patients diagnosed with adenomyosis who underwent ultrasound-guided HIFU ablation under conscious sedation between July 2021 and July 2023. Patients were randomly allocated into a training set and a test set at a ratio of 7:3. The study aimed to evaluate the distribution of clinical characteristics among patients experiencing effective versus ineffective ablation at two distinct classification thresholds (0.7 and 0.5). Multiple models were developed to explore the combination of effective radiomic features derived from dual-sequence MRI and clinical data. Radiomic features were extracted from the MRI images of adenomyosis lesions in the training set. This process included feature extraction, selection, model construction, and evaluation. Logistic regression was used to construct the predictive model, and its performance was assessed on the test set using the receiver operating characteristic (ROC) curve. The Delong test, net reclassification improvement (NRI), and integrated discrimination improvement (IDI) were used to compare the predictive accuracy of the models.

Results: The predictive model showed better alignment with actual ablation outcomes, particularly for predicting ablation success rates exceeding 50%. The combination of radiomic features from the two MRI sequences achieved an AUC of 0.84 in the test set. Decision curve analysis demonstrated that the combined model provided greater net benefit than the single-sequence radiomics model across a broader range of risk thresholds. For the prediction of 70% efficacy, the combined model achieved an AUC of 0.804 in the test set, slightly lower the 50% efficacy prediction task.

Conclusion: The model, based on dual-sequence MRI radiomics, emerges as a promising tool for predicting the efficacy of HIFU ablation, potentially aiding clinicians in anticipating the outcomes of HIFU ablation procedures.

Keywords: adenomyosis, high-intensity focused ultrasound, ablation, radiomics analysis, magnetic resonance imaging

Introduction

Adenomyosis is a prevalent gynecological disorder affecting women of reproductive age, with an incidence rate ranging from 7% to 23%.[1] The disorder is characterized by the invasion of endometrial tissue into the uterine muscle layer, leading to uterine enlargement, dysmenorrhea, and menorrhagia.[2] Initial diagnosis is primarily based on clinical symptoms, with magnetic resonance imaging (MRI) being the most accurate radiological tool for diagnosing adenomyosis.[3–5] Adenomyosis treatment

Received: 27 December 2024
Accepted: 25 April 2025
Published: 9 May 2025

options include pharmacotherapy, surgical intervention, and interventional procedures.[6–11] Although conservative surgery has proven effective in over 50% of patients, long-term follow-up data remains insufficient.[12,13]

High-intensity focused ultrasound (HIFU) is a novel non-invasive treatment modality that uses ultrasound's penetrative, directional, and focal characteristics to induce coagulative necrosis within targeted areas, destroying lesions without damaging surrounding tissues.[14–16] HIFU treatment alleviates symptoms, with its efficacy closely related to immediate postoperative ablation rates.[17]

Imaging biomarkers, such as T2-weighted MR imaging signal intensity, apparent diffusion coefficient, and ultrasound perfusion parameters, are commonly utilized to predict ablation efficacy but with limited accuracy.[18,19] In current clinical practice, the non-perfused volume ratio (NPVR) serves as an index for evaluating HIFU efficacy.[20] Advances in imaging technology, particularly the extraction of imaging features to construct accurate and objective efficacy prediction models, are crucial for the clinical expansion of HIFU, potentially benefiting more patients with adenomyosis.[21] The T2-Fat Suppression (T2FS) sequence provides information on the aqueous components within lesions, helping to identify areas of necrosis or edema, while the T1 contrast-enhanced (T1C) sequence reflects the blood supply and perfusion status of the lesions, aiding in the assessment of the non-perfused region post-treatment.[22,23] In evaluating HIFU ablation efficacy for adenomyosis, the combination of these two sequences offers a comprehensive reflection of the lesion's physical characteristics and treatment response. Specifically, T2FS illustrates structural changes within the lesion, while T1C highlights the blood flow and perfusion status of the tissue after ablation.

Radiomics analysis uses comprehensive methods to quantify texture, shape, and intensity patterns within the tumor region on MRI images. It has been utilized for predicting early recurrence (within 2 years) after curative resection of hepatocellular carcinoma (HCC),[23,24] and for predicting residual myoma regrowth within one year in uterine myomas treated with HIFU ablation.[25] Additionally, previous studies have evaluated the combined predictive value of radiomics based on different MRI sequences in determining the non-perfused volume ratio (NPVR) following HIFU ablation for uterine fibroids.[26–28]

This study primarily investigates the value of radiomics models based on dual-sequence MRI in predicting the efficacy of HIFU ablation in patients with adenomyosis.

Materials and Methods

Patients

The Institutional Review Board approved this retrospective analysis, and informed consent was not required (IRB no. 2024–056). Between July 2021 and July 2023, 188 individuals underwent HIFU ablation at our center. Eligibility for participation included: (1) women between the ages of 18 and the menopausal transition with diagnosed adenomyosis through clinical and radiological assessments; (2) individuals undergoing their initial HIFU ablation for adenomyosis; (3) MRI scans performed within three days prior to and following the ablation; (4) no previous surgical intervention or medical treatment for adenomyosis. Participants were excluded if they had: (1) other identified uterine or adnexal issues; (2) inadequate MRI image quality. A total of 114 patients who completed a one-year follow-up were included in this study for further analysis. Patients were randomly divided into a training set and a test set at a ratio of 7:3. The patient recruitment flowchart is presented in Figure 1.

MR Imaging

Patients underwent examination using a 1.5T MRI scanner (MAGNETOM Aera, Siemens Healthcare, Germany) equipped with a body phased-array coil. The primary imaging sequences selected were axial T2-weighted MR imaging (T2WI) with fat saturation and contrast-enhanced T1-weighted MR imaging (CE-T1WI). The imaging parameters were set as follows: (1) For T2WI with fat saturation, the repetition time (TR) was set at 2500 ms, and the echo time (TE) was set at 88 ms. The slice thickness was 4 mm, the slice spacing was 1.2 mm, and the field of view (FOV) was 260 mm × 260 mm. (2) For CE-T1WI, the TR was set at 6.8 ms, and the TE was set at 2.4 ms. The slice thickness was 3 mm, the slice spacing was 0.6 mm, and the FOV was 260 mm × 260 mm. Dimeglumine gadopentetic acid was administered intravenously at a rate of 2.0 mL/s and a dose of 0.2 mmol/kg via a high-pressure syringe from the superficial vein of the forearm. The injection contained 20 mL of gadobenate dimeglumine, equivalent to 6.680g of gadobenic acid and 3.900g

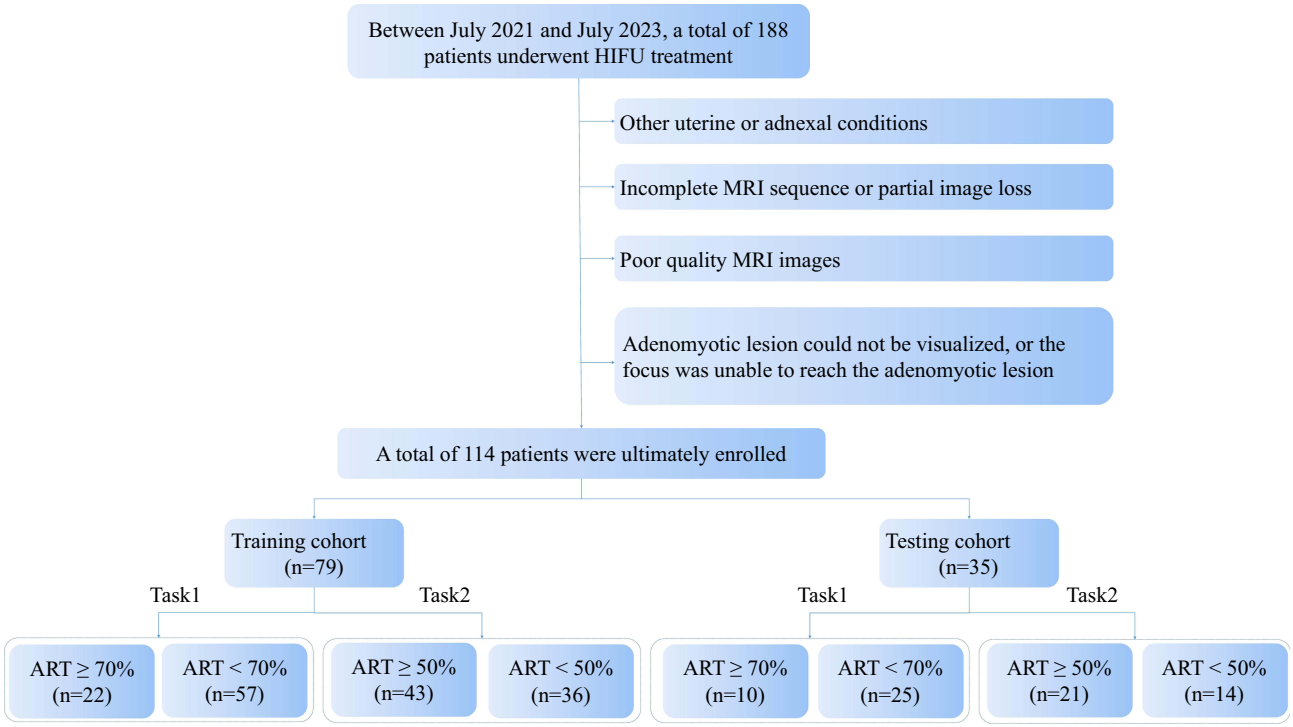

Figure 1 Study flowchart of the enrolled patients with exclusion criteria.

of N-methylglucamine, provided by Shanghai Bolaike Xinyi Pharmaceutical Co., Ltd. CE-T1WI observations were made 35 seconds after the injection.

Image Analysis

All original axial T2WI and CE-T1WI images before and after HIFU treatment were transferred to the offline image workstation. Prior to HIFU treatment, Radiologist 1 (with 5 years of experience in gynecologic tumor diagnosis) manually mapped each patient's T2WI and CE-T1WI layer by layer, following the edge of the relatively low-signal lesions. This mapping referenced the multi-sequence MR enhancement images of the patient's pelvis in the PACS system, with regions of interest (ROIs) encompassing the entire tumor. Following HIFU treatment, Radiologist 1 manually traced the lesion of each patient along the edge of the ablation area (necrotic area), with ROIs covering the entire ablation zone. These ROIs were then reviewed by Radiologist 2 (with 15 years of experience in gynecologic tumor diagnosis).

All patients underwent MRI within 3 days after HIFU to assess the endometrium's condition and evaluate the non-perfused volume (NPV). The volume of the adenomyosis lesion and the NPV were measured on each slice of the contrast-enhanced T1WI. The ablation volume (V) was calculated using the ellipsoid volume formula: $V = (A \times B \times C) / 6$, where A, B, and C represent the length, width, and height of the lesion, respectively.[29] The non-perfused volume ratio (NPVR) was determined as NPV/adenomyosis × 100%. Studies have shown that the efficacy of HIFU ablation for adenomyosis correlates with the NPVR.[30] Previous research has indicated that satisfactory clinical outcomes can be achieved when the NPVR is 50% or higher. Multiple studies have reported that the average or median NPVR for HIFU ablation of adenomyosis ranges from 50% to 70%.[30–33] Therefore, in this study, to identify an optimal model with NPVR thresholds of 50% and 70%, adenomyosis cases in the training and test cohorts were categorized into effective ablation (NPVR ≥ 70% and ≥ 50%) and ineffective ablation (NPVR < 70% and < 50%) cohorts.

Clinical–Radiological Features

Clinical and radiological features that might affect the non-perfused volume ratio (NPVR) of adenomyosis were analyzed. These included age, preoperative blood routine, coagulation function, Carbohydrate Antigen 125 (CA-125),

size and type of adenomyosis lesions, and Color Doppler flow imaging (CDFI) signals. The Visual Analog Scale (VAS) scores and menstrual flow were assessed before and after treatment. The CDFI signal was categorized using the Adler grading system as follows: Grade 0 indicates no short rod or punctate flow signals; Grade I indicates one or two short rods or punctate flow signals; Grade II indicates three to four punctate vessels; Grade III indicates more than four blood vessels or an intertwined network of blood vessels. The VAS score was used to evaluate changes in dysmenorrhea. Menstrual pain was scored on a 0–10 Numerical Rating Scale (NRS), where 0 indicates no pain, 1–3 points indicate mild pain, 4–6 points indicate moderate pain, and 7–10 points indicate severe pain.

Radiomics Analysis

Radiomics analysis,[34] including tumor segmentation, was performed using the uAI Research Portal (uRP, version 231115, United Imaging Intelligence Co., Ltd., China). The workflow for radiomics analysis consists of the following steps: tumor segmentation, feature extraction, feature selection, model construction, model analysis, and evaluation. A flowchart depicting this process is provided in Figure 2.

Tumor Segmentation

For each subject, an abdominal radiologist with 10 years of experience manually delineated the tumor region (volume of interest, VOI) based on dual MR sequences T2FS and T1C). A senior abdominal radiologist reviewed these delineations. To evaluate the reproducibility of radiomics features, 30 patients with adenomyosis were randomly selected and outlined by Radiologist 2. The intra-class correlation coefficient (ICC) was utilized to assess the consistency between the delineations of the two cohorts.

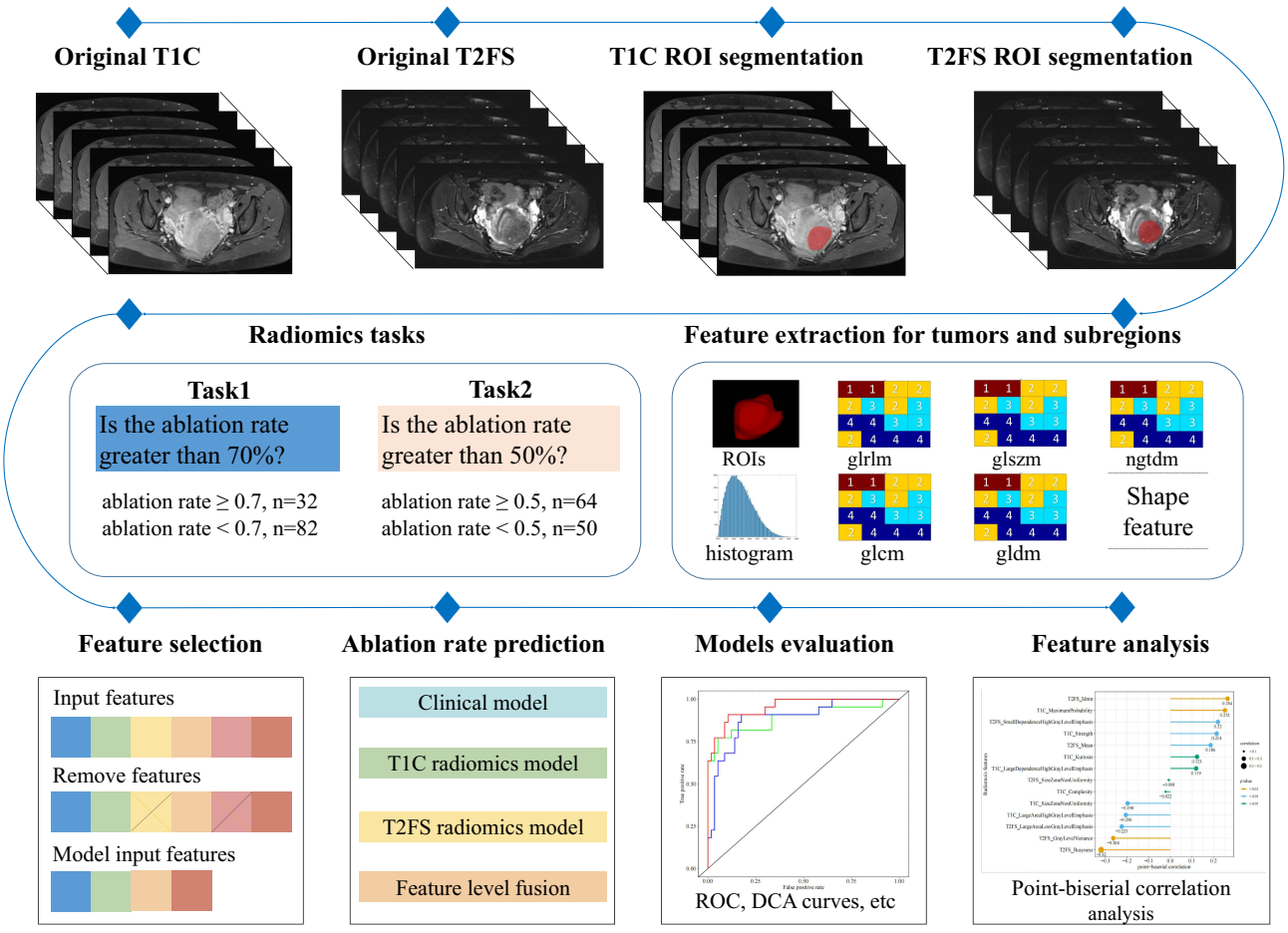

Figure 2 Study flowchart of Radiomics analysis.

Feature Extraction and Selection

To reduce heterogeneity among MR images, all MR images were resampled using bilinear interpolation to achieve an isotropic voxel size of $1 \times 1 \times 1$ mm^3. Subsequently, intensity normalization was performed by applying a fixed bin width of 25 and z-score normalization to achieve a standard normal distribution of image intensities. Radiomics features were extracted using the uAI Research Portal, which integrates PyRadiomics (https://pyradiomics.readthedocs.io/en/v3.0.1/). For each sequence, 2264 radiomics features were extracted and categorized into first-order, shape, texture, and higher-order features (Table S1).

Feature selection was conducted exclusively on the training set to prevent information leakage between the training and test datasets. Radiomics features were first extracted and subsequently normalized using z-score normalization. Following this, features with an intra-class correlation coefficient (ICC) of 0.75 or higher in test-retest evaluations were identified as reproducible and selected for further analysis. Optimal predictive features were then identified through correlation analysis (with a p-value ≤ 0.05) and the least absolute shrinkage and selection operator (LASSO) method.

Model Construction and Evaluation

In both classification tasks, the optimal feature selection results were used to construct five models: clinical model, T1C model (single-sequence radiomics model), T2FS model (single-sequence radiomics model), Radiomics model (combination of T1C and T2FS), and the Combination model (combination of T1C, T2FS, and clinical features). For all fusion models, we employed feature-level fusion, merging the features from the single-sequence models and selecting them for the fusion model. The model's performance was evaluated by generating receiver operating characteristic (ROC) curves and calculating the area under the curve (AUC), as well as metrics for sensitivity, specificity, accuracy, precision, and F1 scores. The Delong test with bootstrap resampling was used to compare predictive efficiency among the models, and false discovery rates (FDR) were adjusted using the Benjamini-Hochberg method. Additionally, the performance of various Radiomics models was assessed using the net reclassification improvement index (NRI) and integrated discrimination improvement index (IDI).

The actual and predicted ablation rates at thresholds of 50% and 70% were evaluated using the Hosmer-Lemeshow test, and calibration curves were plotted. To validate the clinical applicability of Radiomics models, decision curves were constructed to quantify the net benefits under various risk thresholds.

Statistical Analysis

Student's t-tests were conducted for variables with a normal distribution, while the Mann–Whitney *U*-test was used for variables with a non-normal distribution. The chi-square test was applied to qualitative variables to determine statistically significant differences. Univariate and multivariate analyses were employed to identify independent predictors. The statistical analysis was carried out using R software, version 4.1.3. All statistical tests were two-sided, with a p-value of less than 0.05 considered statistically significant.

Results

Clinical–Radiological Features

Clinical and radiological characteristics of all study patients were analyzed using ablation rate thresholds of 70% and 50% (Tables 1 and S2). For predicting an effective ablation rate greater than 50%, univariate analysis identified VAS_BeforeTreatment, Ultrasonic Blood Flow, Uterine Size, and Lesion Size as significant factors. Multivariate analysis showed that VAS_BeforeTreatment and Ultrasonic Blood Flow were independent predictors, with p-values below 0.05. For predicting an ablation rate greater than 70%, Age, VAS_BeforeTreatment, Ultrasonic Blood Flow, and Lesion Size were significant in univariate analysis, while VAS_BeforeTreatment and Ultrasonic Blood Flow remained independent predictors in multivariate analysis.

https://doi.org/10.2147/IJWH.S512216

Table 1 Baseline Clinicoradiological Characteristics of Patients with Adenomyosis in the Training and Testing Cohorts (Ablation Rate Threshold = 70%)

Characteristics	Training Group			Testing Group		
	Negative (n=57)	Positive (n=22)	p	Negative (n=25)	Positive (n=10)	p
Diseases (%)						
Adenomyosis	54 (94.7)	19 (86.4)	0.432	24 (96.0)	8 (80.0)	0.190
Other	3 (5.3)	3 (13.6)		1 (4.0)	2 (20.0)	
Lesion Type (%)						
Focal lesions	20 (35.1)	6 (27.3)	0.508	6 (24.0)	3 (30.0)	0.694
Diffuse lesions	37 (64.9)	16 (72.7)		19 (76.0)	7 (70.0)	
Menstruation Before Treatment (%)						
Moderate	3 (5.3)	2 (9.1)	0.178	2 (8.0)	1 (10.0)	1.000
Light	34 (59.6)	13 (59.1)		11 (44.0)	5 (50.0)	
Heavy	20 (35.1)	7 (31.8)		12 (48.0)	4 (40.0)	
Menstruation After Treatment (%)						
Moderate	13 (22.8)	4 (18.2)	0.298	6 (24.0)	5 (55.6)	0.193
Light	36 (63.2)	16 (72.7)		18 (72.0)	4 (44.4)	
Heavy	8 (14.0)	2 (9.1)		1 (4.0)	0 (0.0)	
Ultrasonic Blood Flow (%)						
I	0 (0.0)	1 (6.2)	0.792	0 (0.0)	0 (0.0)	1.000
II	28 (68.3)	12 (75.1)		9 (56.2)	5 (62.5)	
III	12 (29.3)	2 (12.5)		6 (37.5)	3 (37.5)	
IV	1 (2.4)	1 (6.2)		1 (6.1)	0 (0.0)	
Age (mean±sd)	42.316 ± 4.231	41.455 ± 4.564	0.448	41.36 ± 5.964	41.8 ± 5.073	0.828
VAS Before Treatment (Median[Q1~Q3])	8[6~8]	6[1.25~7.75]	0.017	6[1~8]	6[5~6.75]	0.941
VAS After Treatment (Median[Q1~Q3])	3[1~3]	0.5[0~2]	0.010	0[0~2]	2[1.25~2.75]	0.047
Blood Platelets (Median[Q1~Q3])	272[215~327]	249.5[205.25~296.5]	0.104	264[219~300]	237.5[222.25~259]	0.685
Hemoglobin (Median[Q1~Q3])	119[99~131]	116.5[105.5~123.75]	0.581	114[100~121]	120[110.25~134.25]	0.369
PT (Median[Q1~Q3])	11.4[10.8~12.2]	11.5[10.825~12]	0.943	11.3[10.8~12.3]	11.45[10.05~13.325]	0.826
PT. (Median[Q1~Q3])	115.72[106.7~124.9]	113.35[104.15~115.6]	0.214	118.91[111.2~123.97]	108.68[99.055~125.85]	0.495
INR (Median[Q1~Q3])	0.96[0.9~1.01]	0.95[0.903~0.97]	0.827	0.95[0.91~0.99]	0.95[0.835~1.02]	0.770
APTT (mean±sd)	27.146 ± 2.784	26.991 ± 2.912	0.832	27.668 ± 3.206	28.16± 1.930	0.235
FIB (mean±sd)	2.751 ± 0.438	2.565 ± 0.598	0.194	3.26 ± 2.584	2.792 ± 0.704	0.956
TT (Median[Q1~Q3])	11.4[10.9~11.9]	11.4[11.025~12.275]	0.626	11.3[10.7~11.6]	11.3[10.65~12]	0.913
D.D (Median[Q1~Q3])	0.07[0.07~0.08]	0.07[0.06~0.152]	0.995	0.07[0.07~0.16]	0.07[0.07~0.07]	0.335
CA125 (Median[Q1~Q3])	71.44[40.68~109.95]	50.1[27.732~81.028]	0.159	51.19[31.095~85.635]	48.515[32.235~104.34]	0.515
Uterine Size (Median[Q1~Q3])	189 303.775[132,717.253~222,012.38]	167 714.51[114,288.72~237 746.179]	0.528	255 656.64[176,780.94~309,804.07]	184 455.4[151,356.02~200,968.13]	0.013
Lesion Size (Median[Q1~Q3])	68 451[40,986~117 174]	31 839[23 478~50,658]	0.002	93,655.5[66,838.5~135 222]	80,856[43 719.847~107 829]	0.220

Feature Extraction and Selection Results

In this study, 2264 features were extracted from the T2-FS and T1C sequences. Specific image filters, radiomics features categories and quantity statistics can be found in Table S1. For the intra-cohort correlation coefficient analysis, a threshold of 0.75 was set, resulting in 1827 reproducible radiomics features in T2-FS and 1618 in T1C. Following correlation and Lasso feature selection on the training set, 11 features were identified in both sequences when the ablation rate threshold was set at 70% (see 13). At a threshold of 50%, 14 features remained in T2-FS and 12 in T1C (see Table S3). Figure S1 shows the Lasso path diagrams for the two MR sequences at different ablation rates.

Performance of Models in Ablation Rate Threshold of 50%

In the Clinical model, the AUC achieved on the test set was 0.6, indicating poor performance (see Table 2, Figure 3A and B). The T1C model and T2FS model exhibited similar performance, with test set AUCs of 0.709 and 0.718, respectively. The Radiomics model, which combined T2FS and T1C features (see Table S4) at the feature level, achieved an AUC of 0.840. The Combination model, which incorporated clinical features along with T2FS and T1C, achieved an AUC of 0.738, performing slightly worse than the Radiomics model. However, the Radiomics model did not show a significant improvement over the single MR sequence models in both the training and test sets (Table 3).

Performance of Models in Ablation Rate Threshold of 70%

In the Clinical model, the AUC achieved on the test set was 0.6 (see Table 2, Figure 3C and D). T1C exhibited higher classification efficiency at the model level than T2FS (test AUC in RF: 0.77 vs 0.676, p=0.45). The Radiomics model, which combined T2FS and T1C features at the feature level, achieved an AUC of 0.804. The Combination model, which incorporated clinical features along with T2FS and T1C, achieved an AUC of 0.736, performing slightly worse than the Radiomics model. In both training and test sets, the Radiomics model significantly outperformed the T2-FS model (Delong test p-values were 0.047 and 0.039 as shown in Table 3). However, no significant difference was observed between the fusion and T1C models. (Table 3).

Model Evaluation

The calibration curves based on random forest prediction results displayed a better fit between the predictive model for whether the ablation rate exceeds 50% and the actual ablation rate in both the training set cohort and the test cohort compared to ablation rate surpasses 70% (refer to Figure S2). The p-values for the Hosmer-Lemeshow test on the training and test sets were 0.286, 0.372, 0.269, and 0.112, 0.148, and 0.594 for the T1C, T2FS, and Radiomics model, respectively, based on the Random Forest classifier (task 50%). The decision curves illustrate that the combination model yielded a greater net benefit than the single-sequence model across a wider range of risk thresholds (see Figure 4).

Figure S1 exhibits the correlation analysis between the radiomics features and the prediction label regarding whether the ablation rate exceeds 50%. Table S5 and Figure S3 reveal that eight radiomics features showed significant correlations with the label and exhibited significant differences between the cohort with an ablation rate greater than 50% and the cohort with an ablation rate less than 50%.

Discussion

This study is the first to predict the efficacy of HIFU ablation for adenomyosis based on T1C combined with T2FS radiomics, which will help clinicians judge the difficulty of ablation before surgery, select an appropriate treatment plan for patients, and promote the development of personalized medicine. The prediction model showed better alignment with actual ablation rates when predicting rates exceeding 50%. Combining radiomics features from two MR sequences achieved an AUC of 0.84 in the testing set. The decision curves illustrate that the combination model yielded a greater net benefit than the single-sequence radiomics model across a wider range of risk thresholds.

In evaluating HIFU ablation efficacy for adenomyosis, the combination of these sequences provides a comprehensive view of the lesion's structure and treatment response, with T2FS highlighting structural changes and T1C showing post-

https://doi.org/10.2147/IJWH.S512216

Table 2 Performance of Radiomics Features and Fusion Models in Predicting the Achievement of 50% and 70% Ablation Rates in Adenomyosis Patients

Ablation rates threshold	Models	AUC (95% CI)		Accuracy		Sensitivity		Specificity		Precision		F1-score	
		Train	Test	Train	Test	Train	Test	Train	Test	Train	Test	Train	Test
70%	Clinical	0.79(0.679–0.902)	0.6(0.399–0.801)	0.797	0.600	0.545	0.700	0.895	0.560	0.667	0.389	0.600	0.500
	T1C	0.930(0.867–0.993)	0.770(0.585–0.955)	0.861	0.714	0.864	0.800	0.860	0.680	0.704	0.500	0.776	0.615
	T2FS	0.954(0.914–0.994)	0.676(0.455–0.897)	0.899	0.800	0.864	0.500	0.912	0.920	0.792	0.714	0.826	0.588
	Radiomics	**0.986(0.967–1.000)**	**0.804(0.614–0.994)**	**0.899**	**0.857**	**0.682**	**0.600**	**0.982**	**0.960**	**0.938**	**0.857**	**0.790**	**0.706**
	Combination	0.994(0.985–1)	0.736(0.524–0.948)	0.911	0.800	0.682	0.600	0.999	0.880	0.999	0.667	0.811	0.632
50%	Clinical	0.799(0.702–0.897)	0.6(0.399–0.802)	0.759	0.629	0.884	0.524	0.611	0.786	0.731	0.786	0.800	0.629
	T1C	0.864(0.787–0.941)	0.709(0.528–0.891)	0.772	0.714	0.837	0.857	0.694	0.500	0.766	0.720	0.800	0.783
	T2FS	0.881(0.808–0.953)	0.718(0.548–0.887)	0.823	0.686	0.977	0.524	0.639	0.929	0.764	0.917	0.857	0.667
	Radiomics	**0.889(0.819–0.958)**	**0.840(0.706–0.974)**	**0.810**	**0.771**	**0.721**	**0.762**	**0.917**	**0.786**	**0.912**	**0.842**	**0.805**	**0.800**
	Combination	0.926(0.868–0.983)	0.738(0.557–0.919)	0.873	0.771	0.953	0.81	0.778	0.714	0.837	0.810	0.891	0.810

Notes: Bold values are the performance of the radiomics model, which integrated T2FS and T1C features at the feature level demonstrated strong predictive performance, achieving AUC values of 0.804 (at 70% ablation rate threshold) and 0.840 (at 50% ablation rate threshold).

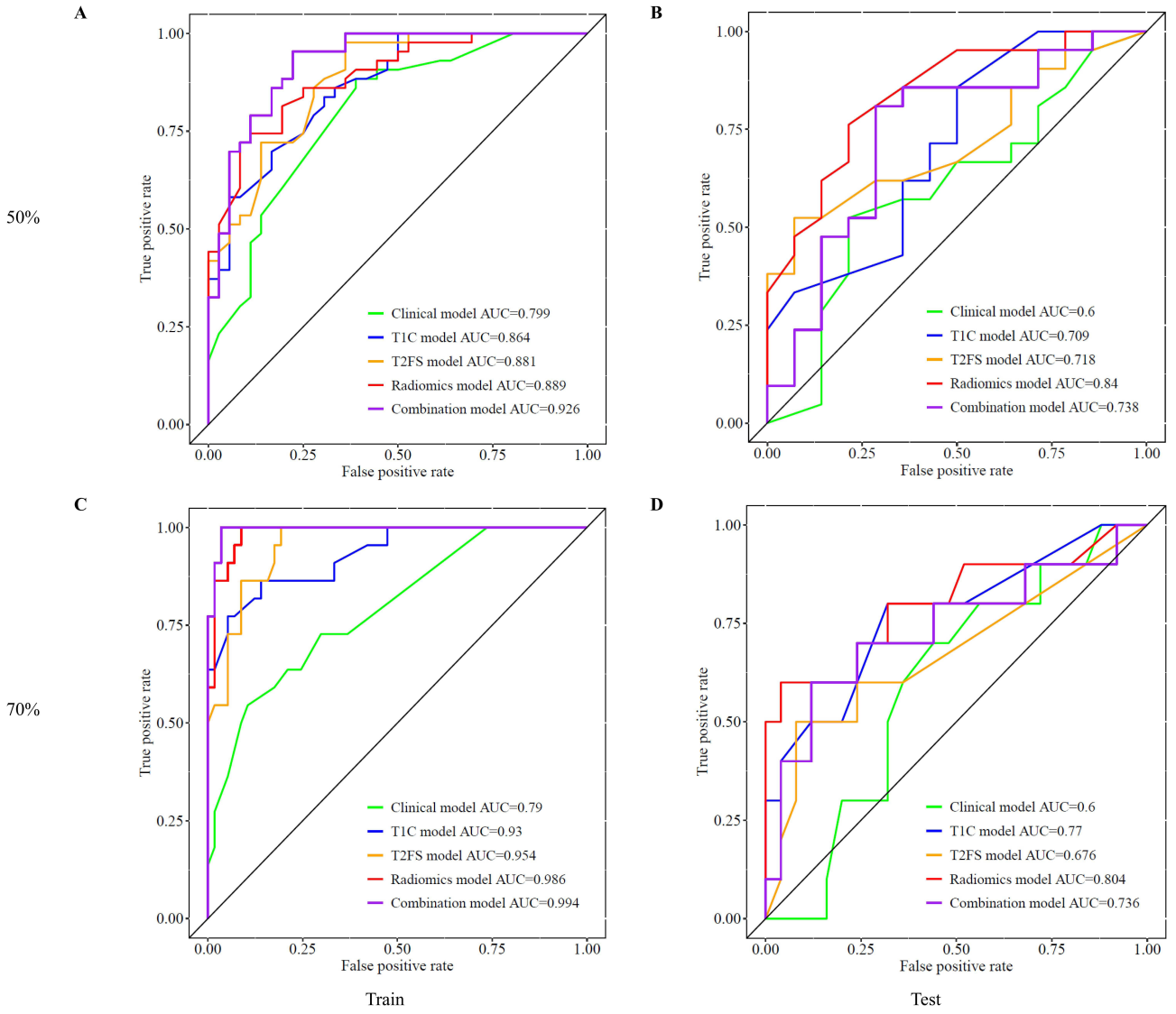

Figure 3 ROC curves for the task of predicting ablation rates greater than 50% and 70%. (**A**, **C**) training cohort, (**B**, **D**) testing cohort.

ablation perfusion status. We included T1C sequences in this study to improve the characterization of adenomyosis by the model, which might also be one of the reasons for the high efficiency of the Radiomics model. Previous studies have also confirmed that the combination of sequences could fully reflect the information of tumors.[35]

Table 3 Comparison of Models in Training and Test Cohorts (Delong Test, NRI and IDI Test)

Ablation rates threshold	Compared models	Basic model	Delong test (p value)		NRI | p value		IDI | p value	
			Training cohort	Testing cohort	Training cohort	Testing cohort	Training cohort	Testing cohort
70%	Radiomics	Clinical	0.001	0.085	**0.416 | 0.001**	**0.580 | 0.001**	**0.382 | < 0.001**	**0.260 | 0.005**
		T1C	0.048	0.682	0.164 | 0.071	0.080 | 0.652	−0.052 | 0.296	−0.024 | 0.772
		T2FS	0.047	0.039	0.151 | 0.087	0.080 | 0.597	0.052 | 0.296	0.024 | 0.772
		Combination	0.359	0.086	0.010 | 0.899	0.120 | 0.065	**0.152 | 0.001**	**0.135 | 0.001**
50%		Clinical	0.128	0.067	0.079 | 0.524	0.405 | 0.064	0.093 | 0.180	0.154 | 0.254
		T1C	0.541	0.173	0.101 | 0.349	0.191 | 0.273	−0.021 | 0.697	0.038 | 0.679
		T2FS	0.877	0.309	0.032 | 0.814	0.238 | 0.307	−0.503 | 0.485	0.064 | 0.550
		Combination	0.166	0.249	−0.066 | 0.532	**0.405 | 0.011**	**0.083 | 0.017**	**0.167 | 0.006**

Notes: Bold values are statistically significant with p<0.05 corrected by false discovery rate (FDR). Net reclassification improvement (NRI) >0 and integrated discrimination improvement (IDI) >0 were positive improvement, indicating that the predictive ability of the new model was better than the old one.

https://doi.org/10.2147/IJWH.S512216

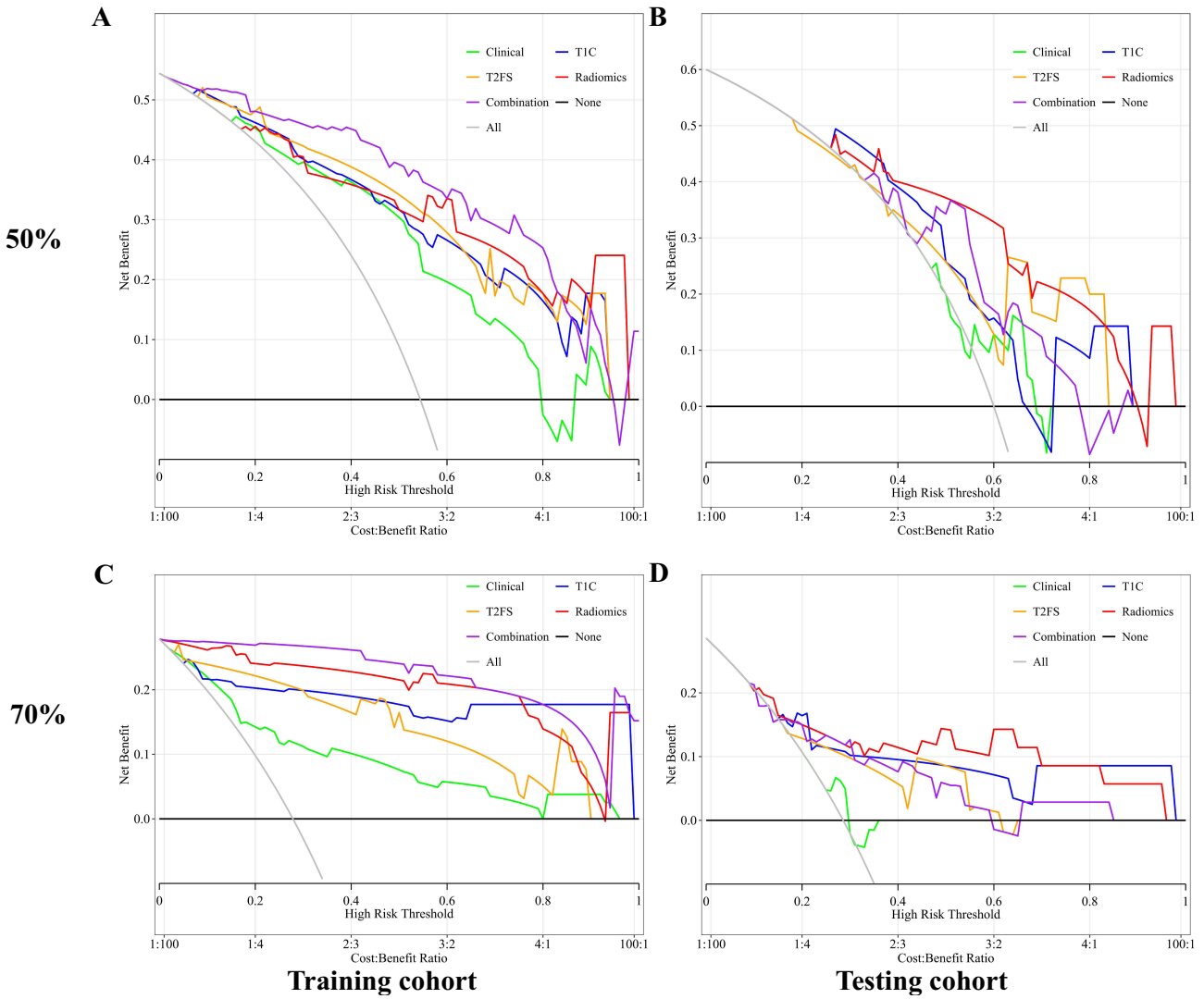

Figure 4 Decision curves for the task of predicting ablation rates greater than 50%. (**A** and **B**) training cohort, (**C** and **D**) testing cohort.

Recent studies have evaluated the value of radiomics models based on non-contrast-enhanced MRI in predicting HIFU ablation efficacy for uterine fibroids.[36,37] They also introduced the potential of dual-sequence MRI radiomics combination models for predicting ablation rates. These combination models demonstrate superior predictive performance compared to radiomics and clinical-radiological models. Similarly, in this study, a clinical model was also developed, but it did not show comparable classification performance to the Radiomics model in either the 50% or 70% efficacy prediction tasks. For the 50% ablation task, the Radiomics model performed better, with volume and texture features (especially gray-level co-occurrence matrix features) showing the strongest correlation with ablation rates and effectively distinguishing treatment outcomes. T2FS signal intensity and morphological features also played a significant role in differentiating effective from ineffective ablation, with signal intensity particularly useful in predicting edema and necrosis. T1C contrast and uniformity were key in identifying areas of effective ablation, potentially helping assess treatment success. The combination of these features provides a more accurate prediction of ablation efficacy, particularly in HIFU treatment for adenomyosis (see Figures S3 and S4).

This study has several limitations worth noting. Firstly, it adopts a single-center retrospective design with a small sample size. Validation through analysis of larger external datasets is required before implementation in clinical settings. Future studies include creating a radiomics model incorporating multiple imaging sequences and clinical information from various centers.

Conclusions

The combination model based on dual-sequence MRI radiomics can be used to predict the efficacy of HIFU treatment for adenomyosis. The results indicate that the combination model yields greater net benefit over single-sequence radiomics models. It was also found that the prediction model for ablation rates greater than 50% will help clinicians better select patients who benefit most from HIFU treatment, provide a reference for treatment decisions, and formulate accurate treatment plans.

Data Sharing Statement

The datasets generated during the current study are included in this published article. Further inquiries can be obtained from the corresponding author.

Ethical Considerations and Data Confidentiality Statement

The Institutional Ethical Committee of Xiangyang Central Hospital waived the requirement for patient consent to review medical records due to the retrospective nature of the study and the de-identification of patient data, which minimizes risks to participant privacy. All patient information used in this analysis was anonymized to ensure confidentiality and comply with the principles outlined in the Declaration of Helsinki. Data access was restricted to authorized personnel, and strict measures were implemented to safeguard against unauthorized disclosure.

Funding

This study has received funding by the Keypoint Research and Development Program of Hubei Province (Grant Number: 2022BCE019), the Key Research & Development Program of Hubei Province (2023BCB128), and Open Fund for the Institute of Gynecological and Obstetric Diseases, Xiangyang City Center Hospital (2023MDI05).

Disclosure

The authors affirm that there were no financial or commercial ties that might be viewed as having a potential conflict of interest for this work.

References

1. Dason ES, Maxim M, Sanders A, et al.. Guideline No. 437: diagnosis and management of adenomyosis. *Journal of Obstetrics and Gynaecology Canada*. 2023;45(6):417–29.e1. doi:10.1016/j.jogc.2023.04.008
2. Bulun SE, Yildiz S, Adli M, et al.. Adenomyosis pathogenesis: insights from next-generation sequencing. *Human Reproduction Update*. 2021;27(6):1086–1097. doi:10.1093/humupd/dmab017
3. Movilla P, Morris S, Isaacson K. A systematic review of tissue sampling techniques for the diagnosis of adenomyosis. *Journal of Minimally Invasive Gynecology*. 2020;27(2):344–351. doi:10.1016/j.jmig.2019.09.001
4. Tellum T, Nygaard S, Lieng M. Noninvasive diagnosis of adenomyosis: a structured review and Meta-analysis of diagnostic accuracy in imaging. *Journal of Minimally Invasive Gynecology*. 2020;27(2):408–18.e3. doi:10.1016/j.jmig.2019.11.001
5. Munro MG. Classification and reporting systems for adenomyosis. *Journal Min Inv Gynecol*. 2020;27(2):296–308. doi:10.1016/j.jmig.2019.11.013
6. Guo SW, Groothuis PG. Is it time for a paradigm shift in drug research and development in endometriosis/adenomyosis?*Human Rep Update*. 2018;24(5):577–598. doi:10.1093/humupd/dmy020
7. Vavilis D, Agorastos T, Tzafetas J, et al.. Adenomyosis at hysterectomy: prevalence and relationship to operative findings and reproductive and menstrual factors. *Clinical and Experimental Obstetrics & Gynecology*. 1997;24(1):36–38.
8. Parazzini F, Mais V, Cipriani S, et al.. Determinants of adenomyosis in women who underwent hysterectomy for benign gynecological conditions: results from a prospective multicentric study in Italy [J]. *European Journal of Obstetrics, Gynecology, and Reproductive Biology*. 2009;143(2):103–106. doi:10.1016/j.ejogrb.2008.12.010
9. Kho KA, Chen JS, Halvorson LM. Diagnosis, evaluation, and treatment of adenomyosis. *JAMA*. 2021;326(2):177–178. doi:10.1001/jama.2020.26436
10. Bakhtiyarov K, Bobrov B, Lubnin D, et al.. Role of uterine artery embolizationb in organ-preserving treatment of adenomyosis (review)]. *Georgian Medical News*. 2022;323:30–37.
11. Grow DR, Filer RB. Treatment of adenomyosis with long-term GnRH analogues: a case report. *Obstetrics and Gynecology*. 1991;78(3 Pt 2):538–539.
12. Wood C. Surgical and medical treatment of adenomyosis. *Human Reproduction Update*. 1998;4(4):323–336. doi:10.1093/humupd/4.4.323
13. Banu NS, Manyonda IT. Alternative medical and surgical options to hysterectomy. *Best Practice & Research Clinical Obstetrics & Gynaecology*. 2005;19(3):431–449. doi:10.1016/j.bpobgyn.2005.01.006
14. S BJ, Y LJ, H CH, et al.. Optimized treatment parameter by computer simulation for high-intensity focused ultrasound treatment of uterine adenomyosis: short-term and long-term results. *PLoS One*. 2024;19(3):e0301193. doi:10.1371/journal.pone.0301193

15. Patel N, Chaudhari K, Patel D, et al.. High-Intensity focused ultrasound ablation of uterine fibroids: a review. *Cureus*. 2023;15(9):e44680. doi:10.7759/cureus.44680
16. Wu S, Liu J, Liu X, et al.. High-intensity focused ultrasound for endometrial ablation in adenomyosis: a clinical study.. *Frontiers in Medicine*. 2024;11:1332080. doi:10.3389/fmed.2024.1332080
17. Machtinger R, Inbar Y, Cohen-Eylon S, et al.. MR-guided focus ultrasound (MRgFUS) for symptomatic uterine fibroids: predictors of treatment success. *Human Reproduction*. 2012;27(12):3425–3431. doi:10.1093/humrep/des333
18. Jacobs MA, Herskovits EH, Kim HS. Uterine fibroids: diffusion-weighted MR imaging for monitoring therapy with focused ultrasound surgery--preliminary study. *Radiology*. 2005;236(1):196–203. doi:10.1148/radiol.2361040312
19. L ZD, X LX, Q TJ, et al.. The value of acoustic radiation force impulse imaging in preoperative prediction for efficacy of high-Intensity focused ultrasound uterine fibroids ablation. *International Journal of Hyperthermia*. 2020;37(1):423–429. doi:10.1080/02656736.2020.1758803
20. Li S, W MW, J YM, et al. Long-term re-intervention after USgHIFU and prediction of NPVR in different ages of patients with uterine fibroids. *International journal of Hyperthermia*. 2024;41(1):2304264. doi:10.1080/02656736.2024.2304264
21. C LP, Rai V, Price N, et al.. Ultrasound-Guided high intensity focused ultrasound ablation for symptomatic uterine fibroids: preliminary clinical experience. *Ultraschall in der Medizin (Stuttgart, Germany: 1980*. 2020;41(5):550–556. doi:10.1055/a-0891-0729
22. Ni M, Wang L, Yu H, et al.. Radiomics approaches for predicting liver fibrosis with nonenhanced T(1) -Weighted Imaging: comparison of different radiomics models. *Journal of Magnetic Resonance Imaging*. 2021;53(4):1080–1089. doi:10.1002/jmri.27391
23. He L, Li H, A DJ, et al.. Machine learning prediction of liver stiffness using clinical and T2-Weighted MRI radiomic data. *AJR American Journal of Roentgenology*. 2019;213(3):592–601. doi:10.2214/AJR.19.21082
24. Chong H, Gong Y, Pan X, et al.. Peritumoral dilation radiomics of gadoxetate disodium-enhanced MRI excellently predicts early recurrence of hepatocellular carcinoma without macrovascular invasion after hepatectomy. *Journal of Hepatocellular Carcinoma*. 2021;8:545–563. doi:10.2147/JHC.S309570
25. Zhou Y, Zhang J, Chen J, et al.. Prediction using T2-weighted magnetic resonance imaging-based radiomics of residual uterine myoma regrowth after high-intensity focused ultrasound ablation [J]. *Ultrasound in Obstetrics & Gynecology*. 2022;60(5):681–692. doi:10.1002/uog.26053
26. Wei C, Li N, Shi B, et al.. The predictive value of conventional MRI combined with radiomics in the immediate ablation rate of HIFU treatment for uterine fibroids. *International Journal of Hyperthermia*. 2022;39(1):475–484. doi:10.1080/02656736.2022.2046182
27. Li C, He Z, Lv F, et al. An interpretable MRI-based radiomics model predicting the prognosis of high-intensity focused ultrasound ablation of uterine fibroids. *Insights Into Imaging*. 2023;14(1):129. doi:10.1186/s13244-023-01445-2
28. Qin S, Jiang Y, Wang F, et al.. Development and validation of a combined model based on dual-sequence MRI radiomics for predicting the efficacy of high-intensity focused ultrasound ablation for hysteromyoma [J]. *International Journal of Hyperthermia*. 2023;40(1):2149862. doi:10.1080/02656736.2022.2149862
29. Li J, Wang W, Liao L, et al.. Analysis of the nonperfused volume ratio of adenomyosis from MRI images based on fewshot learning [J]. *Physics in Medicine and Biology*. 2021;66(4):045019. doi:10.1088/1361-6560/abd66b
30. W YJ, J YM, Jiang L, et al. Factors influencing USgHIFU ablation for adenomyosis with NPVR ≥ 50 [J]. *International Journal of Hyperthermia: the Official Journal of European Society for Hyperthermic Oncology, North American Hyperthermia Group*. 2023;40(1):2211753. doi:10.1080/02656736.2023.2211753
31. Shui L, Mao S, Wu Q, et al.. High-intensity focused ultrasound (HIFU) for adenomyosis: two-year follow-up results. *Ultrasonics Sonochemistry*. 2015;27:677–681. doi:10.1016/j.ultsonch.2015.05.024
32. Jiang Z, Li Q, Li W, et al.. A comparative analysis of pregnancy outcomes of patients with uterine fibroids after high intensity focused ultrasound ablation and laparoscopic myomectomy: a retrospective study [J]. *International Journal of Hyperthermia*. 2021;38(1):79–84. doi:10.1080/02656736.2021.1874547
33. Keserci B, Duc NM. Magnetic resonance imaging parameters in predicting the treatment outcome of High-intensity focused ultrasound ablation of uterine fibroids with an immediate nonperfused volume ratio of at least 90. *Academic radiology*. 2018;25(10):1257–1269. doi:10.1016/j.acra.2018.01.022
34. Wu J, Xia Y, Wang X, et al.. uRP: an integrated research platform for one-stop analysis of medical images. *Frontiers in radiology*. 2023;3:1153784. doi:10.3389/fradi.2023.1153784
35. Zhao Y, Wang N, Wu J, et al.. Radiomics analysis based on contrast-enhanced MRI for prediction of therapeutic response to transarterial chemoembolization in hepatocellular carcinoma. *Frontiers in Oncology*. 2021;11:582788. doi:10.3389/fonc.2021.582788
36. Cheng Y, Yang L, Wang Y, et al.. Development and validation of a radiomics model based on T2-weighted imaging for predicting the efficacy of high intensity focused ultrasound ablation in uterine fibroids [J]. *Quantitative Imaging in Medicine and Surgery*. 2024;14(2):1803–1819. doi:10.21037/qims-23-916
37. Zheng Y, Chen L, Liu M, et al.. Nonenhanced MRI-based radiomics model for preoperative prediction of nonperfused volume ratio for high-intensity focused ultrasound ablation of uterine leiomyomas [J]. *International Journal of Hyperthermia*. 2021;38(1):1349–1358. doi:10.1080/02656736.2021.1972170